Available online at www.sciencedirect.com

ScienceDirect

Procedia Engineering 10 (2011) 2851–2856

Engineering Procedia

ICM11

Characterisation of the Thermal Damage in a Martensitic Steel Substrate Consequent to Laser Cladding Process

B. Valsecchi[a,]*, B. Previtali[a], E. Gariboldi[a], A. Liu[a]

[a]*Politecnico di Milano – Dipartimento di Meccanica, via La Masa 1, Milan 20156, Iatly*

Abstract

The paper deals with the study of the thermal damage of the substrate during the laser cladding process. The laser cladding process is known as a process which causes small thermal damage in the base material situated directly below the deposited powder. However when the laser cladding process is applied to martensitic steels, that have been previously treated in order to obtain well balanced hard and tough structures, the deposition of the heated powder as well as the interaction of the laser beam with the surface can modify the base material properties beneath the cladding layer. As a consequence uncontrolled, different and variable in hardness microstructures are produced. A 1 kW fiber laser source transmitted trough a 50 µm delivery fiber was employed to deposit a common Co-base powder over a martensitic stainless steel. Different process conditions were tested in order to reproduce different temperature fields in the base material. The temperature field in the substrate was measured making use of micro-thermocouples able to capture the fast heating and cooling thermal cycles during the deposition process. The microstructure analysis of the heat affected zones beneath the cladding layer together with the microhardness measurements allowed the thermal damage in terms of extension and intensity to be characterized and compared with the corresponding thermal cycles.

© 2011 Published by Elsevier Ltd. Open access under CC BY-NC-ND license.
Selection and peer-review under responsibility of ICM11

Keywords: active fiber laser cladding, martensitic stainless steel, multi-tracks

1. Introduction

Martensitic stainless steels (MSS) are commonly used for fabricating components that demand high strength and high resistance to wear and corrosion in sectors such as well drilling and oil extraction, mining machinery, thermoelectric plant and steam turbine. For many of these applications, an increase in surface hardness and wear resistance can be beneficial for improving the performance and extending the service life. Various surface modification techniques, such as plasma nitriding, laser surface melting, hardening and cladding, have gained increasing acceptance in recent years [1-3]. Laser cladding in particular has well recognized advantages such as the usable of various powder mixture, low dilution, and smaller distortion [4-5]. By the appearance of the high-power active fiber laser and adequate optics and head devices, a new effective method is offered for the laser cladding of MSS [6].

In the present work the quality of the multi-track laser cladding layer and the thermal damage introduced by the laser cladding in the MSS substrate is investigated when an innovative active fiber laser source is used in conjunction with a specifically designed laser head.

* Corresponding author. Tel.: +39 02 2399 8538; fax: +39 02 2399 8585.
E-mail address: bruno.valsecchi@mecc.polimi.it.

1877-7058 © 2011 Published by Elsevier Ltd. Open access under CC BY-NC-ND license.
Selection and peer-review under responsibility of ICM11 doi:10.1016/j.proeng.2011.04.474

2. Experimental procedure

2.1. Experimental setup

The laser system used for the experimental campaign was a 1 kW IPG active fiber laser transmitted trough a 50 μm delivery fiber. A Sulzer Metco powder feeder was used for supplying the powder into the coaxial channels of the laser head. The used laser cladding head, designed and produced at SITEC- Laboratory for Laser Applications, is characterized by three important items: i) three process gases contemporaneously managed, ii) coaxial design of all head chambers, iii) very compact structure (see the external view in Figure 1a). The coaxial configuration was chosen, due to its asymmetric configuration that is ideal when closed tracks, such as circle paths, have to be clad and due to its compactness. Three different paths for the process gas were obtained. As Figure 1b shows, gas A has two aims: 1) to protect the glass under the focusing lens; 2) to modify the molten pool. The other gases are B and C, the first one is responsible of the powder delivery to the melting pool, which is managed directly by the powder feeder. On the other hand, the gas C is responsible of the shielding of the cladding area. Besides gas C also acts on the powder cone and favours its converge toward the central point, thus the powder is concentrated on the melting point avoiding powder waste and loss of process efficiency. Figure 1c shows the powder cone shape acquired by a high speed CCD camera when the gas C comes out to the external head nozzle.

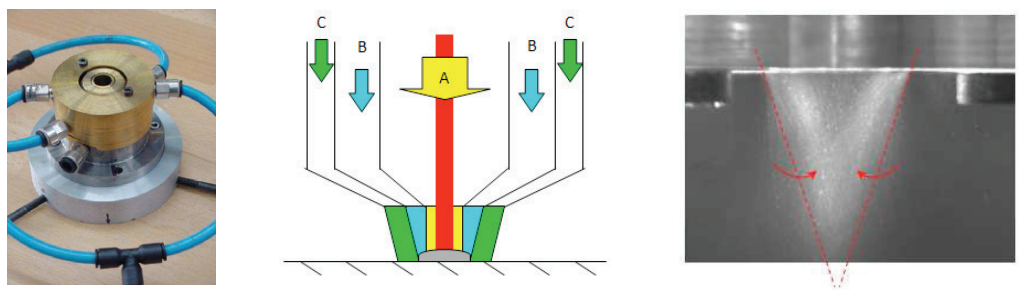

(a) (b) (c)

Fig. 1. (a) Three gases cladding head; (b) Gas head scheme; (c) Effects of gas C on the powder coming out of the nozzle;

During laser cladding the temperature of the workpiece was measured making use of several micro-thermocouples. The micro-thermocouples were uncoated K type, with a wire dimension of 0.5 mm (estimated time constant $\tau_K = 0.125$ s). The acquisition frequency of each thermocouple was 3.6 Hz. The micro-thermocouples were firstly obtained by spot laser welding from the two wires. Then they were fixed by capacitive discharge spot welding on the bottom of two pockets milled on the workpiece according to the scheme of Figure 2 left.

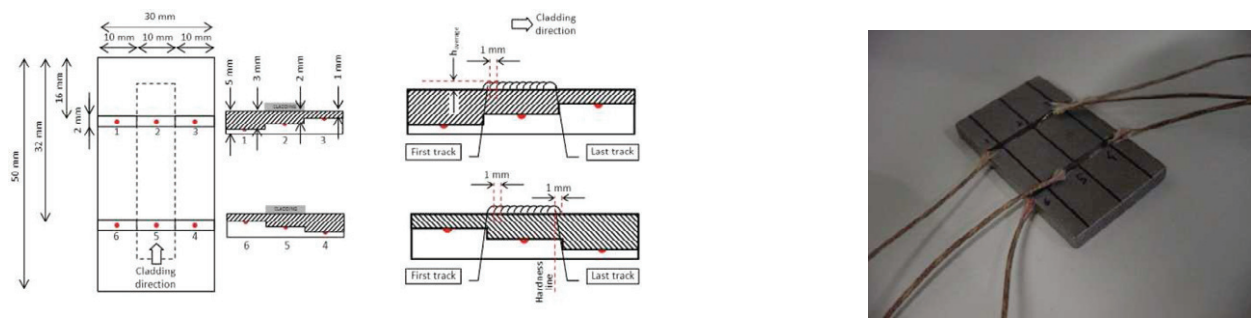

Fig. 2. (a) Scheme of the micro-thermocouples and hardness line position (left); (b) Macroview of the workpiece together with thermocouples (right)

2.2. Material

The substrate material was an AISI 410 stainless steel grade corresponding to the European EN X12Cr steel, characterized by nominal carbon and chromium content of 0.12 and 13 wt.%, respectively. The material, a

martensitic-ferritic steel, was supplied in the annealed condition. The used powder for laser cladding was a Co-base powder, 80-100 μm in size and a spherical appearance to the scanning electron microscopy (SEM). Table 1 presents the powder chemical composition obtained by the EDX microanalysis probe of the SEM .

Table 1. Measured chemical composition of the used Co-based powder (wt%)

C	O	Si	Cr	Ni	Fe	W	Co
2,4	1	2	13	14,6	2	5	Bal.

2.3. Arrangement of the experiment

After a preliminary experimentation, here not reported for the sake of briefness, the laser cladding process parameters were chosen in order to provide optimum coating quality and to investigate two cladding conditions: high input energy and low input energy. To obtain these two conditions the laser scanning speed was changed while all the other parameters were fixed (see Table 2). In particular, all gases in the laser head were nitrogen. The laser beam was defocused to produce a spot diameter of 2 mm. Ten overlapping 45 mm long tracks were made at 50% overlap (1 mm inter-axis, see Figure 2 left) to cover a surface area of 10x45 mm.

Table 2. Fixed and variable process parameters to obtain two process conditions at high and low energy

		Power [W]	Scanning speed [mm/s]	Powder feed rate [g/min]	Stand off distance [mm]	Spot diameter [mm]	Energy [J]
Condition	Low Energy	750	4	10	15	2	25.3
	High Energy	750	3	10	15	2	33.8

After cladding, each sample was cut transversally to the cladding direction in order to obtain samples for metallographic analyses. Two samples were obtained, the first one in correspondence of the position of the first milled pocket, the second one at a distance of about 16 mm from the first one, in correspondence of the second pocket (see Figure 2 left), to check the repeatability of the geometrical and microstructural features along the cladding direction. The cross-section samples were mounted in resin, conventionally polished for metallographic investigations and finally etched using Kalling's n°1 reagent (1.5gr CuCl2, 33 ml ethanol, 33 ml water, 33 ml HCl). This etchant revealed microstructures of both clad and substrate materials. The microstructural features of the samples were analyzed both by Light Optical Microscopy and Scanning Electron Microscopy, in latter case combining the information supplied by different probes, among which the EDX microanalysis to obtain chemical profiles.

On each sample two sets of Vickers hardness tests (0.49N load on the indenter) were performed on a line located within the last tenth track at about 1 mm from its edge (see the hardness line profile in Figure 2 left).

The height of the cladding layer was also measured as well as the temperature profiles obtained by the micro-thermocouples were compared with the hardness values and microstructural analysis.

3. Results and Analysis

The energy transferred to the workpiece E_{abs} during the two cladding conditions can be evaluated as:.

$$E_{abs} = \alpha \frac{P}{v} L \tag{1}$$

where P is the laser power, v the scanning speed, α the absorption coefficient, here set at 30% as suggested in [7-8] and L the overall track length, that means 45 mm x 10 tracks: L = 450 mm. As shown in Table 1 the energies are 25.3 kJ and 33.8 kJ for the low and high energy condition respectively. The temperature curves consequent to the multi-pass laser cladding in the substrate are shown in Figure 3 in the case of points 5 and 2 that are at the multi-pass at the beginning of the track and at the end respectively (see Figure 2 left). As can be seen in Figure 3 high and low energy conditions produces different temperature fields in the workpiece. First of all, the high energy plot (i.e. the cladding obtained with lower scanning speed) produces higher temperature, since the heating phase reaches 820°C before cooling. Moreover the temperature field is more homogeneous in the clad area, since the initial and

final zones show the same temperature profiles. On the other hand temperatures in the low energy condition are lower and different between the initial and final zones. Point 5 indeed does not reach temperature higher than 600°C, while point 2 comes close to 800°C before starting to cool. Therefore the faster scanning speed that obtains the low energy condition produces a not homogeneous temperature field in the clad area.

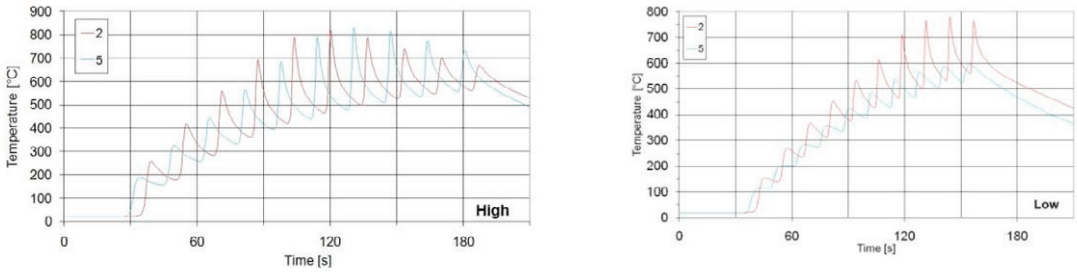

Fig. 3. Temperature profile at points 2 and 5 for high energy condition (left); Temperature at points 2 and 5 for low energy condition (right)

From the microstructural point of view, three main zones can be identified on the cross section of the clad samples: clad zone, heat affected zone (HAZ) and substrate. The macroviews obtained in correspondence of thermocouple at point 5 are shown in Figure 4. As can be seen the cross sections reveal good homogeneity and uniformity of the clad layer that is crack and pore free with strong metallurgical bonding to the substrate in both low and high energy conditions. On the other hand the clad height depends on the process conditions: in the case of low energy the cladding layer is lower and almost homogeneous (from 400 to 500 μm from the first to the tenth track). In the case of high energy conversely the clad height is significantly higher, even the powder feed rate was the same, due to the high input energy that allowed a more efficient powder melting. Beside the clad height increase moving from the first (597 μm) to the eight (1688 μm) and to the tenth track (1016 μm).

The clad zone is characterized by the dendritic solidification structure, with primary dendrites of the FCC Co-rich matrix. This latter is coarser in the high energy condition samples, suggesting lower solidification and cooling rate (see Figure 5). Dendritic structures on the cross-section extend in some cases from the interface to the external surface. Even at higher magnification deleterious features for laser clad layers, such as the presence of small cracks or of porosities were not observed. Within the overlapping regions, i.e. the layers of clad material heated during the following, adjacent cladding track, sometimes micropores were found. Moreover, the complex heat treating cycles left a narrow region of irregular, fragmented dendrites displaying coarsened secondary dendrite arms. They clearly appear both in macrographs and micrographs (Figure 5) particularly in the high energy sample, where elsewhere the cladding region is characterized by very long dendrites.

The region of clad/HAZ interface is characterized by the presence of two layers. On the clad side, a homogeneous layer, with a bright appearance both in optical (Figure 5) and SEM (Figure 6) micrographs is found (6.3 and 5 μm thick in high and low energy condition respectively). This layer is characterized by a chemical composition that is substantially the same for both samples. It also does not significantly different from that of the clad material, but its slightly high iron content suggests the dilution of the substrate material into the closer region of the molten cladding alloy. The composition of the second layer (the thickness of which reached 30 and 35 μm for the high and low energy conditions respectively), roughly corresponds to that of the HAZ/ substrate material. The interface between these two layers has been considered as the interface between the clad and substrate materials. Compositional and hardness profiles are here given referring to it.

The hardness profiles were obtained by means of indentations perpendicularly aligned to the clad/HAZ interface in the last-track portion of the clad zone, where macrographic analyses revealed the maximum extension of the HAZ. Such profiles are shown in Figure 7. The hardness of the Co-base clad alloy, although scattered by the presence of different phases, was of about 500 HV. These values, slightly increased in the case of low energy sample, correspond to those reported in literature for clad layers of the same alloy material [9].

In the monophase region of the HAZ closer to the interface, peak hardness values higher than 600HV were reached in both conditions. Farther from the interface, in the dual phase region characterizing most of the HAZ, the hardness profile differs for the two samples. From its peak values, the hardness of high energy sample decreases to

about 250 HV where remains almost constant for about 2 mm from the interface, where it gradually reach the 170 HV hardness (typical hardness value for the AISI 410 steel in annealed condition).

Fig. 4. Cross-section samples at high energy (sample above) and low energy (sample below).

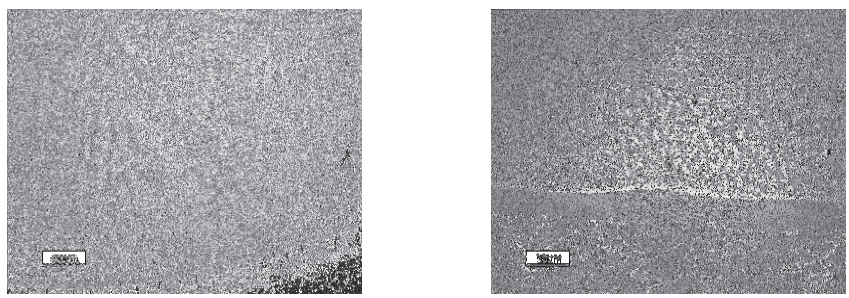

Fig. 5. Microstructural features of the clad layer close to the interface in the cross-section of high (left) and low energy condition samples

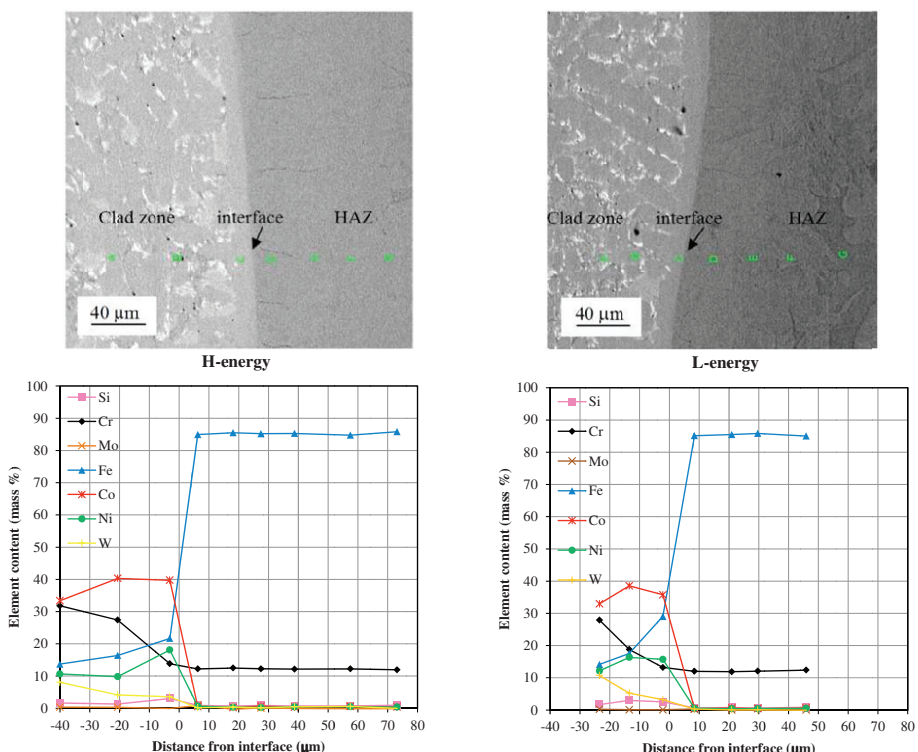

Fig. 6. SEM microstructural features in the region closer to the clad alloy/HAZ interface (above) and corresponding composition profiles of selected alloy elements (below) in the clad and HAZ of high and low energy sample (left and right respectively). The distance from the interface is positive moving toward the HAZ/substrate material.

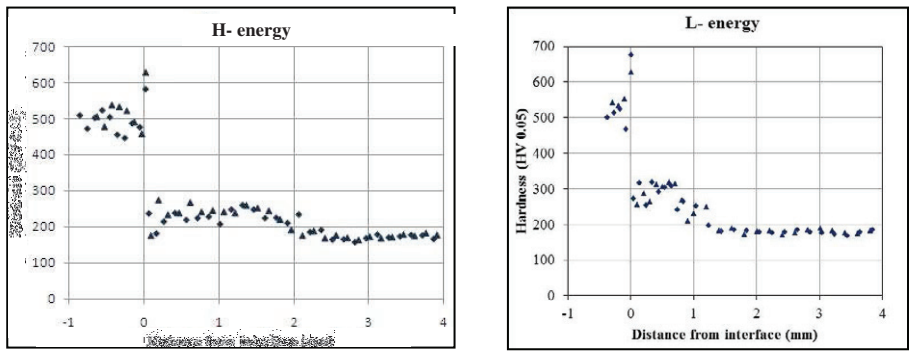

Fig. 7. Hardness profiles taken perpendicularly to the clad/HAZ interface in correspondence of point 5. Plots for high and low energy samples are on the left and right, respectively. The distance from the interface is positive moving toward the HAZ/substrate material.

The hardness profile of the low energy sample was characterized by a thinner plateau at slightly higher hardness (at about 300 HV). In this sample, where the heat input during cladding was lower, the hardness of the initial substrate condition is then reached at about 1.2 mm from the interface.

4. Conclusions

Making use of a recent active fiber laser source and of a specifically designed laser head has allowed obtaining good quality, crack- and pore-free cladding layers of a Co-base powder with strong metallurgical bond on AISI 420 stainless steel. The metallurgical characteristics of the clad layer and of the substrate as well as the clad height were investigated when the input energy varied. The heat input mainly affected the extension of the HAZ as well as the height of the clad layer, since the temperature fields recorded by micro-thermocouples positioned in the substrate showed different heating phases in case of high or low energy inputs. On the other hand the clad integrity was preserved and the dilution was minimum.

References

[1] Wu K, Liu G Q, Wang L, Xu B F. Research on new rapid and deep plasma nitriding techniques of AISI 420 martensitic stainless steel. *Vacuum* 2010; **84**: 870–875.

[2] Mahmoudi B, Torkamany MJ, Sabour AR, Sabbaghzade J. Laser surface hardening of AISI 420 stainless steel treated by pulsed Nd:YAG laser. *Materials and Design* 2010; **31**: 2553–2560.

[3] Vamsi Krishna B, Bandyopadhyay A. Surface modification of AISI 410 stainless steel using laser engineered net shaping. *Materials and Design* 2009; **30**: 1490–1496

[4] Zhang D, Zhang X. Laser cladding of stainless steel with Ni–Cr3C2 and Ni–WC for improving erosive–corrosive wear performance. *Surface & Coatings Technology* 2005;**190**: 212–217.

[5] Xu G, Kutsuna M, Liu Z, Yamada K. Comparison between diode laser and TIG cladding of Co-based alloys on the SUS403 stainless steel. *Surface & Coatings Technology* 2006; **201**: 1138–1144

[6] Valsecchi B, Previtali B, Vedani M, Vimercati G. Fiber laser cladding with high content of wc-co based powder. *Int J Mater Form* 2010; **3(1)**: 1127–1130

[7] Toyserkani E, Khajepour A, Corbin S. 3-D finite element modeling of laser cladding by powder injection: effects of laser pulse shaping on the process. *Optics and Lasers in Engineering* 2004;**41**: 849–867.

[8] Oliveira U, Oceĺık V, De Hosson J. Analysis of coaxial laser cladding processing conditions. *Surface & Coatings Technology* 2005; **197**: 127–136.

[9] Ganesh P, Moitra A. Fracture behavior of laser-clad joint of Stellite 21 on AISI 316L stainless steel, *Materials Science and Engineering*; 2010 **527**(16-17): 3748-3756